Title

Single-cell RNA sequencing reveals immunological rewiring at the maternal-fetal interface following asymptomatic/mild SARS-CoV-2 infection

Journal

Cell Reports, 39(11)

ISSN

2639-1856

Authors

Sureshchandra, Suhas

Zulu, Michael Z

Doratt, Brianna M

et al.

Publication Date

2022-06-01

DOI

10.1016/j.celrep.2022.110938

Since January 2020 Elsevier has created a COVID-19 resource centre with free information in English and Mandarin on the novel coronavirus COVID-19. The COVID-19 resource centre is hosted on Elsevier Connect, the company's public news and information website.

Cell Reports

Article

Single-cell RNA sequencing reveals immunological rewiring at the maternal-fetal interface following asymptomatic/mild SARS-CoV-2 infection

Graphical abstract

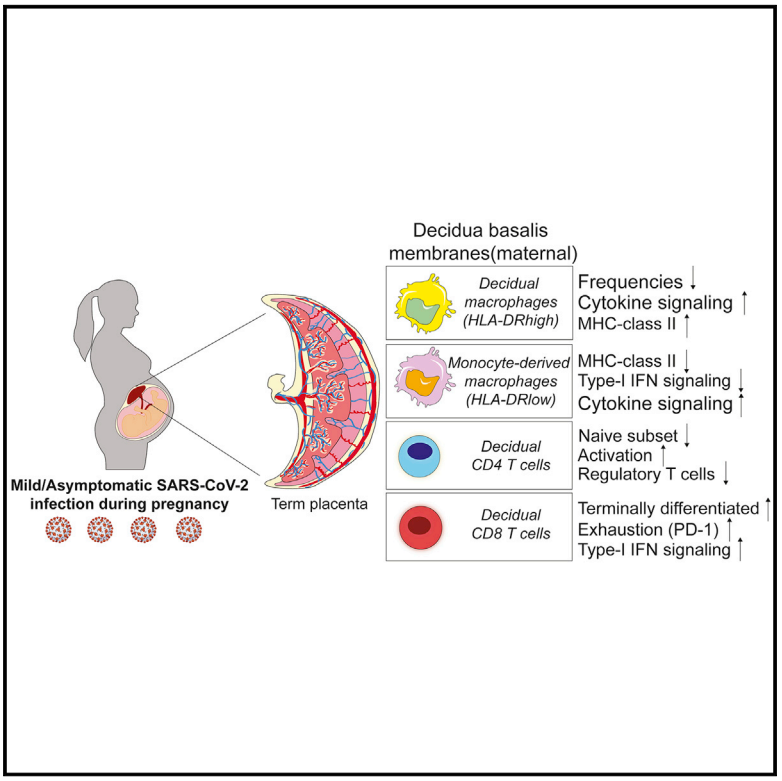

Highlights

- Asymptomatic and mild COVID-19 significantly remodels the maternal-fetal interface
- Altered frequency of decidual macrophages, T regs, and activated T cells
- Antigen presentation and type I IFN signaling are attenuated in decidual macrophages
- T cell repertoire diversity in circulation and decidua is reduced

Authors

Suhas Sureshchandra, Michael Z. Zulu, Brianna M. Doratt, ..., Monica Rincon, Nicole E. Marshall, Ilhem Messaoudi

Correspondence

Ilhem.messaoudi@uky.edu

In brief

Sureshchandra et al. describe extensive changes in blood and decidua obtained from pregnant women experiencing asymptomatic and mild SARS-CoV-2 infection. These data indicate that, regardless of severity, COVID-19 re-models the maternal-fetal interface with potentially significant ramifications for pregnancy and neonatal outcomes.

Sureshchandra et al., 2022, Cell Reports *39*, 110938
June 14, 2022
https://doi.org/10.1016/j.celrep.2022.110938

CellPress

Cell Reports

CellPress
OPEN ACCESS

Article

Single-cell RNA sequencing reveals immunological rewiring at the maternal-fetal interface following asymptomatic/mild SARS-CoV-2 infection

Suhas Sureshchandra,[1,2] Michael Z. Zulu,[1,2] Brianna M. Doratt,[1,2,3] Allen Jankeel,[1] Delia Tifrea,[4] Robert Edwards,[4] Monica Rincon,[5] Nicole E. Marshall,[5] and Ilhem Messaoudi[1,2,3,6,*]

[1]Department of Molecular Biology and Biochemistry, School of Biological Sciences, University of California, Irvine, CA 92697, USA
[2]Institute for Immunology, University of California, Irvine, CA 92697, USA
[3]Department of Microbiology, Immunology, and Molecular Genetics, College of Medicine, University of Kentucky, Lexington, KY 40536, USA
[4]Department of Pathology and Laboratory Medicine, School of Medicine, University of California, Irvine, CA 92697, USA
[5]Maternal-Fetal Medicine, Oregon Health and Sciences University, Portland, OR 97239, USA
[6]Lead contact
*Correspondence: Ilhem.messaoudi@uky.edu
https://doi.org/10.1016/j.celrep.2022.110938

SUMMARY

While severe coronavirus 2019 (COVID-19) is associated with immune activation at the maternal-fetal interface, responses to asymptomatic/mild severe acute respiratory syndrome coronavirus 2 (SARS-CoV-2) infection during pregnancy remain unknown. Here, we assess immunological adaptations in blood and term decidua in response to asymptomatic/mild disease in pregnant women. We report attenuated antigen presentation and type I interferon (IFN) signaling pathways, loss of tissue-resident decidual macrophages, and upregulated cytokine/chemokine signaling in monocyte-derived decidual macrophages. Furthermore, we describe increased frequencies of activated tissue-resident T cells and decreased abundance of regulatory T cells with infection while frequencies of cytotoxic CD4/CD8 T cells are increased in the blood. In contrast to decidual macrophages, type I IFN signaling is higher in decidual T cells. Finally, infection leads to a narrowing of T cell receptor diversity in both blood and decidua. Collectively, these observations indicate that asymptomatic/mild COVID-19 during pregnancy results in remodeling of the immunological landscape of the maternal-fetal interface, with a potential for long-term adverse outcomes for the offspring.

INTRODUCTION

The current pandemic of coronavirus disease 2019 (COVID-19) caused by severe acute respiratory syndrome coronavirus 2 (SARS-CoV-2) continues to be a significant global threat (Huang et al., 2020). Overwhelming evidence suggests that pregnant women are a high-risk group for COVID-19 (Subbaraman, 2021). Indeed, a study on severe COVID-19 infections in pregnant women from 18 countries has reported higher rates of adverse outcomes such as mortality, preeclampsia, and preterm birth (Villar et al., 2021). While pregnant women with a severe COVID-19 diagnosis are at 62% higher odds of getting admitted to the intensive care unit (ICU) compared with non-pregnant women of reproductive age (Subbaraman, 2021; Yap et al., 2020), a majority of those who get exposed to the virus experience asymptomatic or mild COVID-19 (Edlow et al., 2020b; Li et al., 2020; Lokken et al., 2020; Panagiotakopoulos et al., 2020). Both vulnerability and immune responses to viral infections during pregnancy can be distinct compared with non-gravid individuals, as observed in influenza, hepatitis E, varicella, and measles (Jamieson et al., 2006; Kourtis et al., 2014; Sappenfield et al., 2013). These differences are primarily driven by peripheral immune adaptations during pregnancy (Aghaeepour et al., 2017, 2018) that balance fetal tolerance and growth with host defense. A recent analysis of the peripheral immune system of mothers with asymptomatic disease revealed an increase in low-density neutrophils (LDNs) but no gross changes in leukocyte frequencies, activation, or function (De Biasi et al., 2021). Furthermore, the cytokine storm that is characteristic of severe COVID-19 in the general population is hardly reported in cases of severe COVID-19 among pregnant patients (Hojyo et al., 2020; Wang et al., 2020). These findings support the hypothesis that pregnancy limits the induction of exuberant peripheral inflammatory responses to SARS-CoV-2 infection that are widely reported in non-pregnant individuals.

The immunological landscape of the maternal-fetal interface (placenta) undergoes significant changes during pregnancy. The decidual compartments of the placenta harbor maternal immune cells (macrophages, natural killer [NK] cells, and T cells [Vento-Tormo et al., 2018]), which exhibit mixed signatures of activation and regulatory phenotype that correlate with gestation (van der Zwan et al., 2018) and can respond to foreign particles at the maternal-fetal interface (Ander et al., 2019). However, details of decidual adaptations to a respiratory infection such as

COVID-19 are slowly beginning to emerge. Although available data strongly suggest a lack of vertical transmission (Edlow et al., 2020b; Garcia-Flores et al., 2021; Schwartz and Morotti, 2020; Vivanti et al., 2020) with rare detection of viral RNA in the placenta (Edlow et al., 2020a), severe COVID-19 has been shown to trigger maternal inflammatory responses at the maternal-fetal interface (Garcia-Flores et al., 2021; Lu-Culligan et al., 2021). Specifically, an increase in markers associated with preeclampsia and activation of placental NK cells and T cells and increased expression of interferon-related genes and stress-associated heat-shock proteins have been reported (Lu-Culligan et al., 2021). However, placental immune rewiring with asymptomatic/mild infections and how that relates to peripheral immune adaptations remain poorly understood.

Therefore, in this study, we examined the effect of maternal asymptomatic/mild SARS-CoV-2 infection occurring during late pregnancy on peripheral and decidual immune cells of the maternal-fetal interface at term. We used single-cell RNA sequencing and multicolor flow cytometry to profile changes in the immune landscape of maternal decidua. Our analysis revealed an expansion of CD69+ T cells and selective loss of HLA-DR^{high} regulatory macrophages and regulatory T cells (Tregs) with asymptomatic/mild SARS-CoV-2 infection in the decidua. Single-cell analysis revealed broad activation of myeloid cells in the decidua, with enrichment of cytokine-secreting subsets, attenuation of interferon signaling, and a concomitant drop in expression of major histocompatibility complex (MHC) class II molecules in blood monocyte-derived macrophage subsets. Activated T cells and terminally differentiated CD8 T cells (TEMRAs) were enriched with infection, but an expansion of cytotoxic CD4 and antiviral CD8 T cells was only observed in the blood. While cytokine-signaling modules were attenuated in the blood, elevated interferon-signaling signatures were detected in the decidua. These findings highlight that even asymptomatic/mild infection can trigger placental immune activation with potential long-term consequences for the developing fetus.

RESULTS

Peripheral and decidual immunological changes in response to asymptomatic/mild SARS-CoV-2 infection

To comprehensively assess the impact of asymptomatic/mild SARS-CoV-2 infection on the immune landscape of the maternal-fetal interface, we collected decidua basalis (maternal membrane) and blood at delivery from mothers who experienced mild symptoms consistent with an upper respiratory tract infection not requiring medical care during pregnancy and had a positive SARS-CoV-2 PCR+ (mild) or those who tested positive during mandatory screening at the time of delivery but experienced no symptoms (asymptomatic) (Figure 1A; Table S1). We observed no differences in antibody titers ($p = 0.599$ for NP immunoglobulin G [IgG] and $p = 0.87$ for receptor-binding domain [RBD] IgG) between subjects in the mild and asymptomatic groups. Therefore, all subsequent analyses were performed on all SARS-CoV-2-exposed subjects (referred to as the asymptomatic/mild group) and compared with SARS-naïve healthy pregnant subjects (healthy donors [HDs]). No difference in age or body mass index was observed between SARS-CoV-2-exposed subjects and HDs. Blood samples were used to obtain complete blood counts and plasma antibody titers and to assess changes in peripheral immune blood cell (peripheral blood mononuclear cells [PBMCs]) composition by flow cytometry (Figure 1A). Decidual immune cells were phenotyped using multispectral flow cytometry and single-cell RNA sequencing to assess immune perturbations at the maternal/fetal interface.

Complete blood cell counts indicated that absolute numbers of circulating granulocytes, monocytes, and platelets increased with infection, but no changes in lymphocyte numbers were detected (Figure S1A). Multicolor flow analysis of PBMCs (Figure S1B) revealed a redistribution of naive and memory T cell subsets in the absence of changes in total CD4 and CD8 T cell frequencies (Figures S1C and S1D). Specifically, infection status was associated with a reduced abundance of naive CD4 T cells but a modest expansion of central memory T cells (TCMs) (Figure S1D). Similar trends were observed in the CD8 subset, where a modest reduction in naive T cells was accompanied by increased frequency of effector memory (EMs) and effector memory CD45RA+ (TEMRAs) cells (Figure S1D). The frequency of total B cells and relative abundance of naive/memory subsets did not vary significantly with infection (Figure S1E). Although proportions of total NK cells did not vary with infection, the relative proportions of CD16^{br}CD56^{dim} expanded with infection while those of the CD16+CD56+ subset decreased (Figure S1F). Similarly, while frequencies of total monocytes and dendritic cells (DCs) were comparable between the two groups (Figure S1G), a modest expansion of CD16++ non-classical monocytes and a significant drop in plasmacytoid DCs (pDCs) was noted (Figure S1H). Finally, no differences in surface expression of MHC class II molecule HLA-DR (Figure S1I) or activation marker CD86 (Figure S1J) were observed with infection.

Flow analysis of decidual leukocytes revealed no changes in total T or B cell frequencies (Figures 1B and S2A). However, we observed a modest expansion of CD4 EMs and a modest reduction in the CD8 naive T cells (Figure 1C) as well as frequencies of CD69+CD103-CD4 and CD8 tissue-resident T cells with asymptomatic/mild disease (Figure 1D). No differences in total decidual NK cell frequencies or subsets were observed (Figures S2B and S2C). However, proportions of both HLA-DR^{high} macrophages and DCs decreased significantly with asymptomatic/mild infection (Figure 1E).

Unsupervised single-cell analysis of decidual leukocytes reveals heightened myeloid cell activation with asymptomatic/mild SARS-CoV-2 infection

We next assessed the rewiring of immune (CD45+) cell states with asymptomatic/mild infection in an unbiased way at the single-cell resolution. Decidual leukocytes from 4 individuals per group were multiplexed using lipid-tagged oligos (compatible with 3′ single-cell gene expression), sorted to remove dead cells, and analyzed using single-cell RNA sequencing (scRNA-seq) (Figure 1A). Following doublets and dead cell removal, dimension reduction, and clustering, our analysis identified 11 unique immune cell clusters (Figure 2A). Cluster annotations were derived from differential marker analysis (Figure 2B; Table S2) and confirmed using markers previously described for the

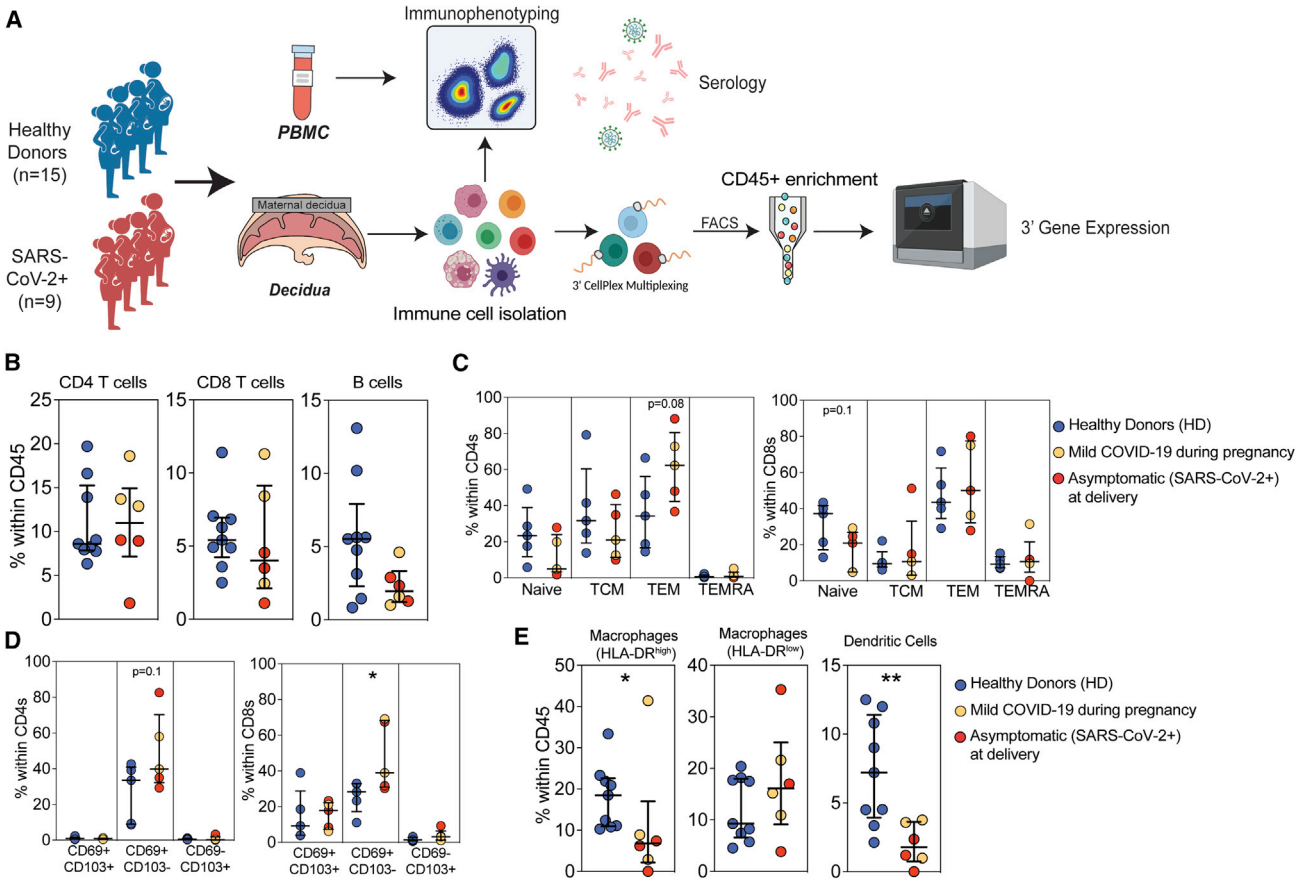

Figure 1. Immunological changes in term maternal decidua with asymptomatic/mild SARS-CoV-2 infection

(A) Experimental design for the study. Placenta and blood were collected from healthy donors (n = 15) and SARS-CoV-2 PCR+ or seropositive pregnant women experiencing asymptomatic/mild disease (n = 9) at delivery. Immunological changes in PBMCs were characterized using multicolor flow cytometry. SARS-CoV-2 specific endpoint titers were measured in plasma using ELISA. Decidual membranes (decidua basalis) were separated from fetal membranes and processed by mechanical and enzymatic methods to isolate immune cells, which were multiplexed and profiled using single-cell RNA sequencing.

(B and C) Dot plots of decidual (B) T and B cells and (C) T cell subsets (naive, central, and effector memory).

(D) Frequencies of tissue-resident CD4 and CD8 T cell subsets characterized by CD69 and CD103 expression.

(E) Dot plots of frequencies of innate immune cells (macrophages and DCs) within the CD45 compartment of decidua basalis of healthy donors (n = 9) and SARS-CoV-2-exposed donors (n = 6). Two group differences were tested using an unpaired t test with Welch's correction. Error bars represent median values and interquartile ranges (*$p < 0.05$; **$p < 0.01$).

first-trimester decidual immune landscape (Vento-Tormo et al., 2018). Within the lymphoid clusters, B cells were identified based on high expression of *CD79A*; CD4 T based on *IL7R* levels; CD8 T on *CD8A* and *GZMH* expression; Tregs on *FOXP3* and *CTLA4* expression; proliferating T cells on *CD2*, *CD3*, and *MKI67* expression; and NK cell subsets on differential expression of *CSF1*, *GZMH*, *CXCR4*, and *ITGB2* (Vento-Tormo et al., 2018) (Figures 2A and 2B; Table S2). Myeloid clusters consisted primarily of macrophages, which were broadly divided by the magnitude of *HLA-DRA* expression (as observed in flow cytometry; Figure S2A; Table S2) into dMac1 (*HLA-DR*^{high}) and dMac2 (*HLA-DR*^{low}) (Vento-Tormo et al., 2018) and DCs, expressing high *FCER1A* (Figures 2A and 2B; Table S2).

We next stratified clusters by SARS-CoV-2-exposure status (Figures 2C and S3A) and patient of origin (since the cells from each subject were barcoded using oligo-tagged lipids) and compared cluster frequencies between the two groups (Figure S3B). No changes were observed in the relative frequency of decidual T cells (Figures S3C and S3D), B cells (Figure S3E), or NK cells (Figure S3F). Additional analysis shows a modest increase in dNK2 (Vento-Tormo et al., 2018) (Figure S3G); therefore, we identified genes differentially expressed with SARS-CoV-2 infection within decidual NK cells. Modest gene-expression changes (73 upregulated and 33 downregulated with infection) were identified with pathways associated with protein folding, MAPK signaling, and type I interferon signaling upregulated with infection, whereas those associated with immune activation and adhesion were downregulated (Figure S3H).

Interestingly, and in contrast to the flow-cytometry data presented above, no differences in DC frequencies were detected from the scRNA-seq data (Figure S3I). However, as observed with flow cytometry, we observed a selective loss of *HLA-DR*^{high} macrophages (dMac1) with asymptomatic/mild SARS-CoV-2 infection (Figure 2D). Additional investigation on this subset

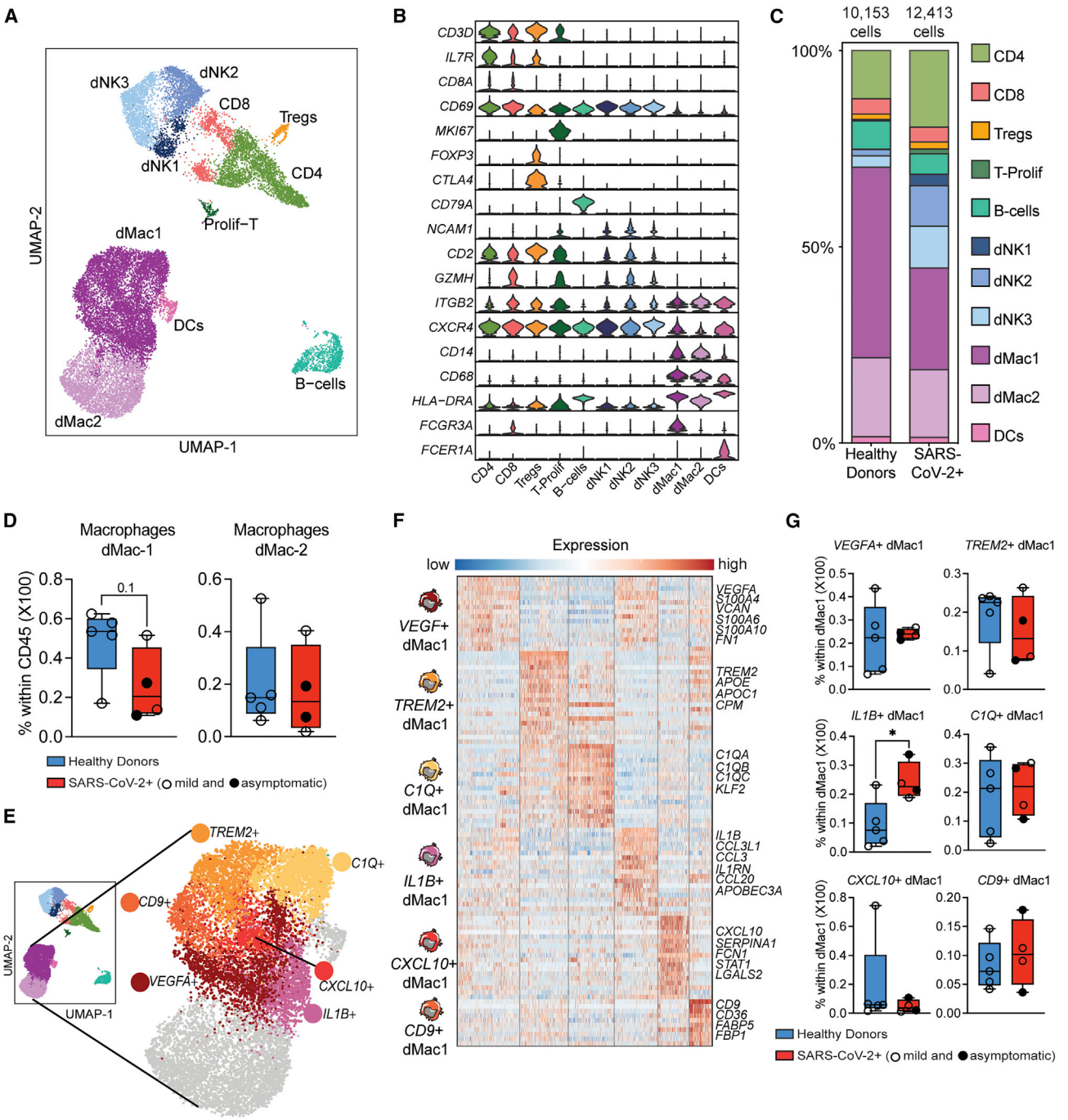

Figure 2. Unsupervised analysis of CD45+ compartment within term maternal decidua and adaptations with asymptomatic/mild SARS-CoV-2 infection

(A) Uniform manifold approximation and projection (UMAP) representation of 22,566 immune cells within the term decidual CD45+ compartment showing 11 clusters.

(B) Violin plots of key gene markers used for cluster annotations. The y axis represents the normalized transcript counts.

(C) Stacked bar graph comparing the distribution of decidual immune cell clusters in healthy donors (n = 5, 10,153 cells) and mothers with asymptomatic/mild SARS-CoV-2 infection (n = 4, 12,413 cells).

(D) Box and whiskers comparing single-cell frequencies of two macrophage subsets dMac1 and dMac2 with asymptomatic/mild SARS-CoV-2 infection.

(E) UMAP of term decidual myeloid cells highlighting the diverse states within the dMac1 (*HLA-DRA*^{high}) macrophage subset. Each color indicates one of 6 dMac1 clusters identified with a prominent marker highlighted.

(legend continued on next page)

revealed a high degree of heterogeneity, with the presence of 6 distinct macrophage states (Figure 2E). These included regulatory macrophages expressing *TREM2* and activated subsets expressing high levels of complement gene *C1Q*, tetraspanin *CD9*, pro-inflammatory cytokine *IL1B*, chemokine *CXCL10* (IP-10), or growth factor *VEGFA* (Figures 2E and 2F).

Although frequencies of dMac1 were reduced with infection (Figure 2G), the *IL1B*+ dMac1 subset expressing cytokines *IL1B*, *CCL3*, and *CCL20* expanded with infection (Figure 2G). Moreover, robust gene-expression changes were observed within both macrophage subsets in response to infection (Figure 3A). In dMac1 macrophages, infection was associated with the induction of genes involved in the antiviral response, viral sensing, nuclear factor κB (NF-κB) signaling, and cytokine production, while a small number of genes that play a role in myeloid cell activation and antigen processing and presentation were suppressed (Figure 3B). More robust gene-expression differences were observed in the dMac2 subset (Figure 3A), altering signatures associated with immune activation, upregulating genes involved in chemotaxis, cell death, and interleukin-17 (IL-17) signaling, and suppressing genes involved in antigen processing and presentation (Figure 3C).

We next compared scores for specific signaling pathways across both groups. SARS-CoV-2 infection was associated with an increase in the scores of modules associated with cytokines and chemokine signaling (Figure 3D), notably NF-κB, tumor necrosis factor (TNF), and IL-17 signaling (Figure S4A) as well as pathogen-sensing pathways such as Toll-like receptor (TLR) and RIG-I signaling (Figure S4B). The higher chemokine module score is illustrated by increased expression of several chemokine genes (such as *CCL3*, *CCL3L1*, *CCL4*, *CXCL3*, and *CCL5*), notably in the dMac1 subset (Figures 3D and 3E). Interestingly, only the dMac2 subset exhibited heightened IL-6 STAT signaling (Figure 3D), including an upregulation of inflammatory genes such as alarmins (*S100A8*, *S100A9, S10012*), *TREM1*, and cytokines (*IL1A*, *IL1B*, *IL6*) with infection (Figure 3E). Additionally, only the dMac2 macrophage subset exhibited dampened type I interferon signaling (Figure 3D) with key interferon-stimulated genes (*IFIT2*, *GBP1*, *IRF1*) downregulated with infection (Figure 3F).

Finally, we observed a differential impact of mild infection of MHC signaling in decidual macrophage subsets. Module scores for MHC class II signaling were upregulated in dMac1 but downregulated in dMac2 macrophages (*HLA-DRA*, *HLA-DRB1*, *HLA-DPB1*) (Figures 3D and 3F), while MHC class I signaling was downregulated in both subsets (Figures 3F and 4C). Interestingly, surface expression of activation markers CD40 and CD86 did not change with infection (Figure S4D). On the other hand, a higher expression level of M2 marker CD206 was detected on dMac1 macrophages, and modest increases in interferon receptor IFNAR1 expression were seen on both subsets (Figure S4E).

Expansion of activated CD4 T cells and upregulation of type I interferon signaling in CD4 and CD8 T cells following asymptomatic/mild SARS-CoV-2 infection

To investigate the impact of asymptomatic/mild SARS-CoV-2 infection in pregnant mothers on diverse T cell states within term placentas, we profiled sorted CD3+ T cells from decidual leukocytes and performed single-cell analysis (gene expression and T cell repertoire) following multiplexing and feature barcoding (5′ technology for parallel gene expression and T cell repertoire analyses) while simultaneously staining for CD4, CD8, CD45RA, tissue markers CD69 and CD103, and regulatory markers PD1 and CD25. Orthogonal readouts were measured in T cells from matched blood samples (Figure 4A). After doublets and ambient RNA removal, we identified 10 memory T cell clusters in addition to a naive cluster (Figure 4B; Tables S3 and S4) within the decidua. Both surface expression of CD4, CD8, CD69, CD103, CD25, and PD-1 from feature barcoding (Figure S5A) and highly expressed RNA markers (Figure 4C; Tables S3 and S4), were used to annotate these memory T cell clusters. All memory CD4s expressed CD69, with three additional clusters expressing either high levels of PD-1 or RNA levels of *HLA-DRA* or *KLRB1* (Tables S3 and S4). Memory CD8 T cells, on the other hand, expressed either CD69 (including a subset of gamma delta T cells) or CD103 and PD-1 (including a subset of proliferating CD8s) (Figures 4B, 4C, and S5A; Tables S3 and S4).

We next compared the proportions of decidual T cell clusters with infection (Figures S5B and S5C). A modest reduction in naive T cells and a statistically significant reduction in Treg frequencies were observed with infection (Figures 4D and S5C). This reduction was accompanied by an overall expansion of CD69+ memory subsets (Figures S5C and S5D), as observed with flow cytometry (Figure 1D). Interestingly, a subset of activated CD4+CD69+*HLA-DRA*+ was significantly expanded with infection (Figure 4D). This subset of T cells, which was nearly absent in HDs, expressed high levels of genes involved in the regulation of viral processes, stress response, cell adhesion, and apoptosis (Figure 4E). Differential gene-expression analysis of memory CD4 T cells showed upregulation of *IFNG*, antiviral genes (*OASL*, *ISG155*, *XAF1*), and heat-shock proteins (*HSPA6*, *HSPA8*) but downregulation of Th2 genes (*GATA3*, *PDE4D*) (Figure 4F). Although frequencies of CD8 T cell subsets did not vary significantly with infection (Figure S5E), differential gene expression analysis revealed elevated signatures of T cell apoptosis, viral processes, myeloid leukocyte activation, and antigen processing and presentation (Figures 4G and 4H). On the other hand, genes associated with NF-κB signaling were downregulated with infection (*NFKBIA*, *CCL4*) (Figures 4G and 4H). Finally, increased module scores for IL-2, type I interferon, and T cell signaling, as well as T cell activation and exhaustion, were observed with SARS-CoV-2 infection (Figure S5F).

(F) Heatmap of normalized transcript counts of top 20 genes within each of the 6 dMac1 clusters. A handful of highly expressed markers within each cluster are highlighted. Color in the heatmap represents scaled average expression ranging from low (blue) to high (red).
(G) Box and whiskers comparing changes in macrophage subset frequencies with asymptomatic/mild SARS-CoV-2 infection. Two group differences were tested using an unpaired t test with Welch's correction (*$p < 0.05$).

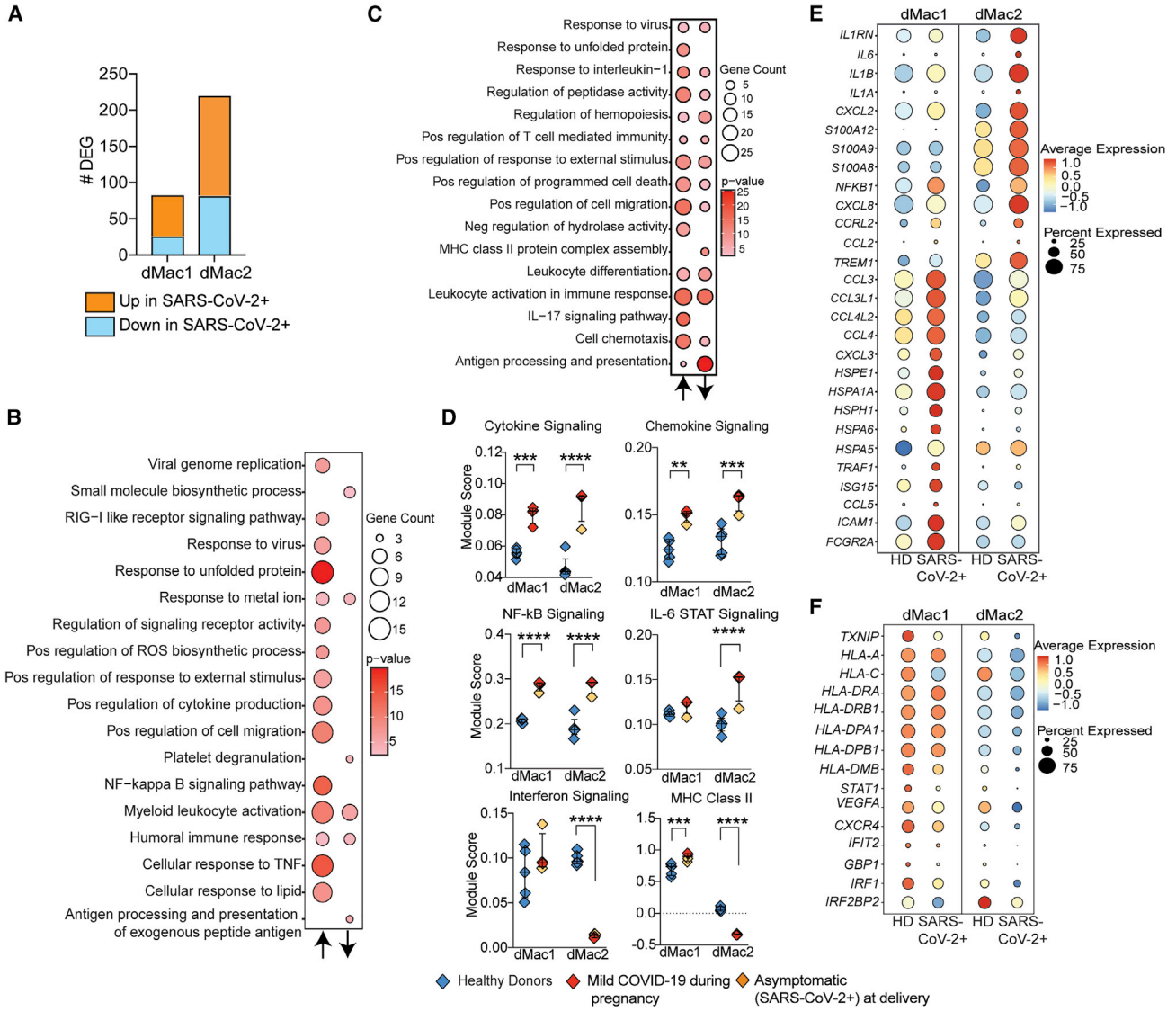

Figure 3. Asymptomatic/mild SARS-CoV-2 infection and associated myeloid cell activation in term decidua

(A) Differentially expressed genes in decidual macrophage subsets with asymptomatic/mild SARS-CoV-2 infection (n = 4 healthy donors; n = 5 asymptomatic/mild SARS-CoV-2 infection).

(B and C) Bubble plots representing two-way functional enrichment of genes up- and downregulated with asymptomatic/mild SARS-CoV-2 infection in (B) dMac1 and (C) dMac2 macrophage subsets. The size of the bubble represents the number of genes mapping to the term, whereas the color represents the level of statistical significance. Two-way enrichments were performed in Metascape.

(D) Dot plots comparing changes in module scores of innate immune pathways in decidual macrophage subsets with asymptomatic/mild SARS-CoV-2 infection. Each dot represents the median module score for the individual. Error bars represent median values and interquartile ranges.

(E and F) Bubble plot depicting normalized expression of key differentially expressed genes (statistically significant adjusted $p < 0.05$ and fold change > 0.4). (E) Upregulated and (F) downregulated with infection. The size of the bubble represents the percentage of cells within the cluster (dMac1 or dMac2) expressing the gene, while the color represents the average expression (normalized transcripts) scaled from low (blue) to intermediate (yellow) to high (red) (**$p < 0.01$; ***$p < 0.001$; ****$p < 0.0001$).

Distinct impact of asymptomatic/mild SARS-CoV-2 infection during pregnancy on peripheral and decidual T cells

We next investigated peripheral T cell adaptations to asymptomatic SARS-CoV-2 infection and compared it with changes observed in placental T cells. Dimension reduction and clustering identified naive, central memory, and several clusters of effector memory T cells, particularly within CD8 EMs (Figure 5A) that were annotated using a combination of gene expression (Figure S6A) and protein markers (Figure S6B). Several clusters of naive CD4 T cells varying in their T cell receptor (TCR) gene usage (*TRA* or *TRB*) were all pooled as a naive CD4 cluster (Figure 5A). We compared frequencies of T cell clusters with infection and analyzed differential gene expression changes within

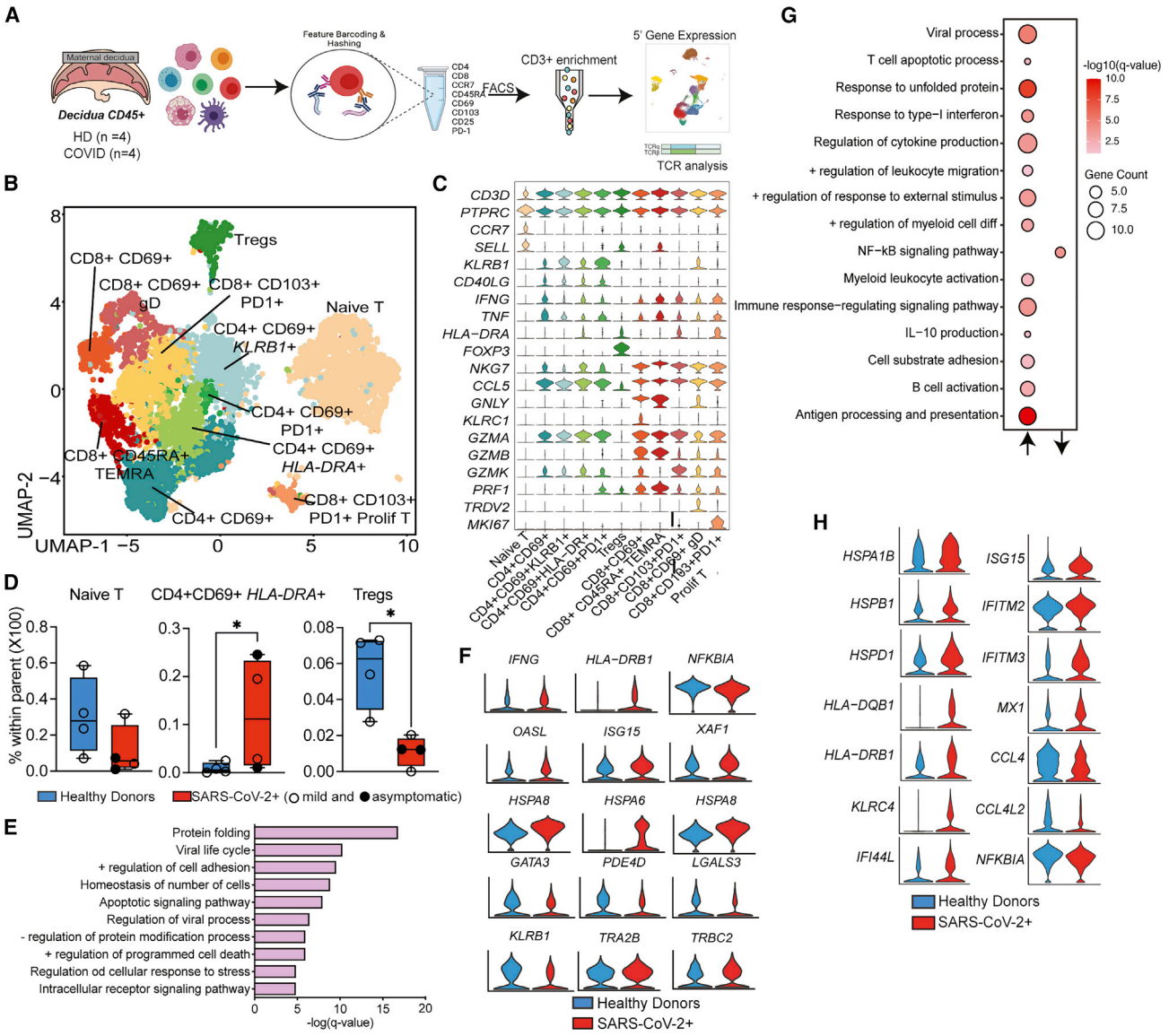

Figure 4. Decidual T cell adaptations to maternal asymptomatic/mild SARS-CoV-2 infection

(A) Experimental design for deep profiling of T cells from blood and maternal decidua (n = 4/group). Isolated immune cells from decidua basalis were surface stained with a fluorescent marker for T cells (CD3), DNA oligo-tagged antibodies for CD4, CD8, naive, and memory, and tissue-resident markers, along with hashing antibodies, enriched for T cells using fluorescence-activated cell sorting (FACS), and subjected to 5′ gene expression and TCR analysis (immune repertoire) on the 10X platform.

(B) Dimension reduction and clustering of decidual T cells identifies 11 distinct T cell clusters at term, annotated by unique surface- and gene-expression markers.

(C) Stacked violin plots highlighting key gene-expression markers of T cell subsets within term maternal decidua. The y axis represents the normalized transcript counts.

(D) Box and whiskers plot of decidual T cell subsets changing with asymptomatic/mild SARS-CoV-2 infection.

(E) Functional enrichment of top genes (log2 fold change $\geq$ 0.4, q value $\leq$ 0.05) within the CD4+CD69+HLA-DRA^{high} T cell cluster. The y axis represents q values (negative log10 transformed).

(F) Violin plots of select statistically significant (log2 fold change $\geq$ 0.4, up- or downregulated, q value $\leq$ 0.05) differentially expressed genes with asymptomatic/mild SARS-CoV-2 infection within memory CD4 T cell clusters.

(G) Bubble plots representing two-way functional enrichment of genes up- and downregulated with asymptomatic/mild SARS-CoV-2 infection in memory CD8 T cell clusters. The size of the bubble represents the number of genes mapping to the term, whereas the color represents the level of statistical significance.

(H) Violin plots of select statistically significant (log2 fold change $\geq$ 0.4, up- or downregulated, q value $\leq$ 0.05) differentially expressed genes with asymptomatic SARS-CoV-2 infection within memory CD4 T cell clusters. Two group differences were tested using an unpaired t test with Welch's correction (**p < 0.01; ***p < 0.001; ****p < 0.0001).

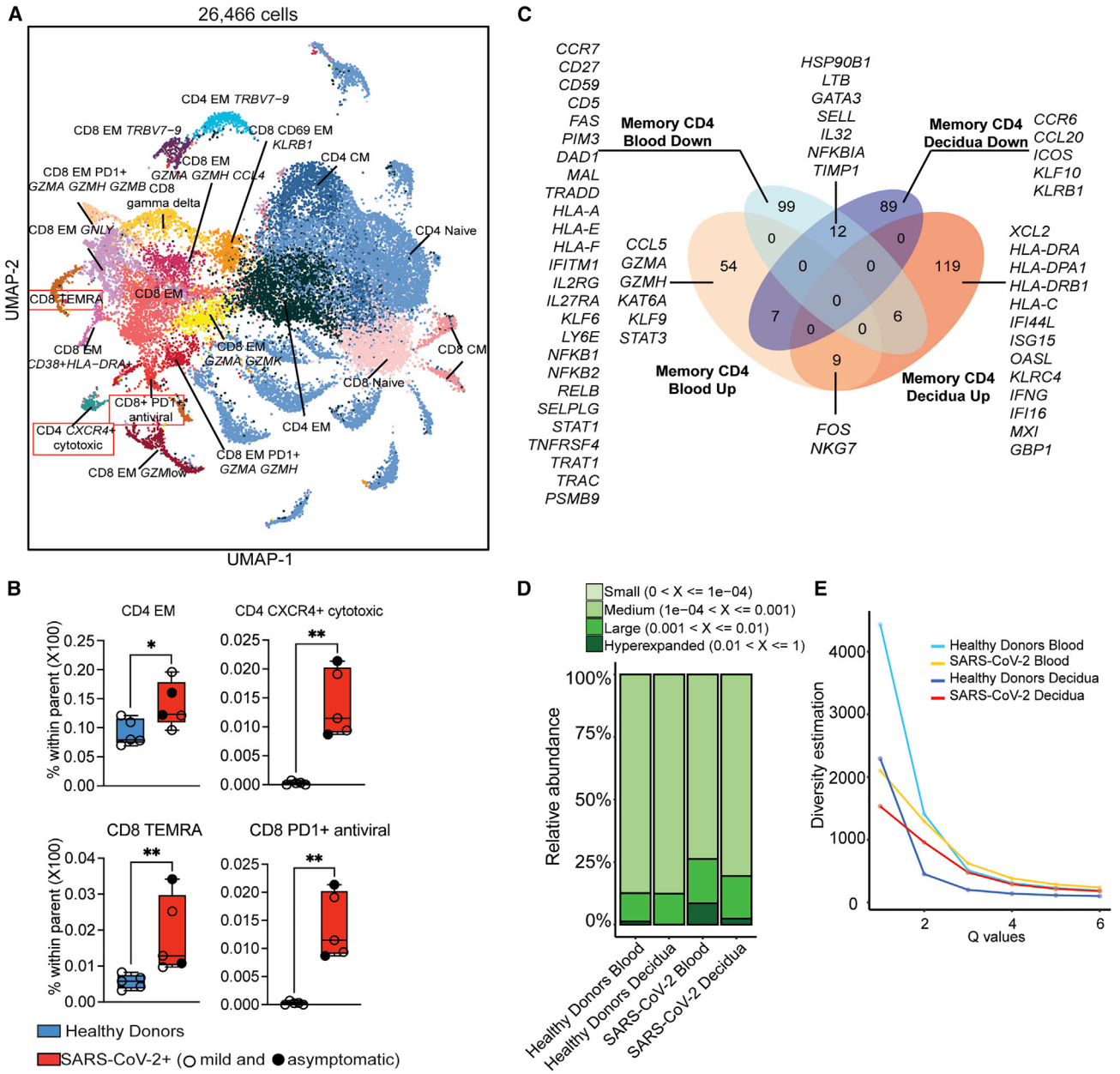

Figure 5. Comparing decidual T cell responses with asymptomatic/mild infection to adaptations in blood

(A) Dimension-reduced UMAP representation of 26,466 blood T cells collected during delivery (n = 4/group)—12,819 from healthy donors and 13,647 from mothers with asymptomatic/mild SARS-CoV-2 infection. Key clusters are annotated based on top gene expression and protein markers identified by Seurat.

(B) Box and whiskers plot of key blood CD4 (top) and CD8 (bottom) T cell subsets changing with asymptomatic SARS-CoV-2 infection.

(C) Venn diagram comparing differentially expressed genes (log2 fold change ≥ 0.4, up- or downregulated, q value ≤ 0.05) in memory CD4 T cells from blood and decidua. Select genes within this comparison are highlighted.

(D) Stacked bars comparing T cell clone sizes (based on proportions within clonal T cells) in blood and decidua in healthy donors and mothers with asymptomatic/mild infection.

(E) Diversity profiles of T cells with infection—y axis represents Hill diversity, interpreted as the effective number of clonotypes within the dataset (*p < 0.05).

total memory T cells. Within CD4 T cells, this analysis revealed an expansion of EMs and a cluster of CXCR4+ cells expressing cytotoxic molecules with infection (Figure 5B). Differentially expressed genes with infection in the blood were quite distinct from ones observed in decidua (Figure 5C). For example, while decidual T cells exhibited upregulation of antiviral (*IFI44L*, *ISG15*, *OASL*, *IFNG*, *MX1*, *GBP1*) and MHC class II signaling (*HLA-DRA*, *HLA-DRB1*), matched blood T cells exhibited elevated cytotoxic signatures (*CCL5*, *GZMA*, *GZMH*). More importantly, genes associated with apoptotic (*FAS*, *PIM3*,

DAD1, *MAL*, *TRADD*), TNF (*CD27*, *TNFRSF4*, *STAT1*), and TCR signaling (*TRAT1*, *TRAC*, *PSMB9*) were exclusively downregulated in blood CD4 T cells (Figure 5C).

Within CD8+ T cells, infection was associated with an expansion of TEMRA and PD1+ CD8 T cells expressing antiviral transcripts (Figures 5B and S6C). Additionally, distinct antiviral signatures were upregulated in decidua (*ISG15*, *MX1*, *IFI6*, *IFITM2*) compared with blood (*OASL*, *CXCR4*, *IFIT2*, *TNF*, *TNFAIP3*, *FOS*) (Figure S6D). Infection was associated with the upregulation of MHC class II genes in both decidual and blood CD8 T cells (Figure S6D). However, blood CD8 T cells exhibited profound dampening of cytotoxicity genes such as *GNLY*, *NKG7*, *PRF1*, *KLRD1*, and *KLRK1*. Furthermore, several genes involved in TCR signaling (*CD247*, *LCK*, *TRAC*, *TRAB1*, *CSK*, *UBB*) were significantly downregulated in blood. Finally, clonal analysis of T cells revealed expansion of large clones (>100 cells) with infection in blood but not in decidua (Figures 5D and S6E), where only small clones were detected. Furthermore, T cells repertoire diversity in blood was lower than that of decidual T cells after infection (Figure 5E).

DISCUSSION

Placental immune cells facilitate implantation, fetal growth, and tolerance and promote labor (Vento-Tormo et al., 2018). Immune responses at the maternal-fetal interface are highly fine-tuned, balancing protecting the fetus from pathogens while also limiting excessive inflammatory exposure associated with stress or infection (Ander et al., 2019). *In vitro* studies have demonstrated the ability of the virus to enter ACE2-expressing maternal and fetal cells in the placenta; however, this observation was not recapitulated *in vivo* (Verma et al., 2021). Nevertheless, recent studies have reported immune activation at the maternal-fetal interface with severe COVID-19 in the absence of active infection or viral RNA in the placenta (De Biasi et al., 2021; Lu-Culligan et al., 2021). However, it is currently unclear if the robust immunological changes at the maternal-fetal interface observed with severe disease exist with asymptomatic/mild disease and if these changes are linked to the peripheral immune response to infection. Therefore, in this study, we collected blood and placentas from pregnant mothers who experienced mild SARS-CoV-2 infection during pregnancy or were discovered to be PCR+ during the mandatory screening at the time of delivery with no symptoms of the disease (asymptomatic). Interestingly, a study involving 991 participants concluded that a vast majority of pregnant women with COVID-19 develop an asymptomatic or mild version of the disease, with a more prolonged course of disease compared with infection in non-pregnant women (Afshar et al., 2020). Indeed, our analysis showed that both groups showed comparable antibody titers of anti-SARS-CoV-2 antibodies, perhaps in line with potentially lingering viral RNA in the asymptomatic group. This design allowed us to uncover the impact of asymptomatic/mild SARS-CoV-2 infection on the immunological landscape of maternal decidua and PBMCs using flow cytometry and scRNA-seq.

Mild COVID-19 in the non-gravid population is characterized by lymphopenia, albeit with a lower magnitude than that observed with severe disease (Chen et al., 2020). Patients with mild COVID-19 also experience an early increase in cytokines but a progressive reduction in type I and III interferon responses as well as increased levels of reparative growth factors (Lucas et al., 2020). Furthermore, the increase in innate immune cell frequencies (monocytes, neutrophils, eosinophils) was less dramatic with moderate disease, suggesting a less inflammatory immune response with mild/moderate disease (Lucas et al., 2020). In line with these previous observations, we report elevated frequencies of granulocytes, monocytes, and platelets but with no overt signs of lymphopenia. Moreover, as previously described (Arunachalam et al., 2020; Laing et al., 2020), we show a reduction in pDCs. Finally, we did not observe a redistribution of monocyte subsets or changes in the surface expression of HLA-DR and CD86, similar to a recent report (De Biasi et al., 2021). The minimal immune activation may be driven by the Th2 bias observed with pregnancy (Aghaeepour et al., 2017). Indeed, elevated plasma levels of regulatory IL-1RA and IL-10 were observed in pregnant women with asymptomatic disease (De Biasi et al., 2021). This immune adaptation with pregnancy does not preclude pregnant women from developing an effective adaptive immune response to the virus since T cells from pregnant mothers with asymptomatic disease have been shown to be functionally competent with respect to *ex vivo* cytokine production and proliferation (De Biasi et al., 2021; Hsieh et al., 2022). Similarly, we report a reduction in naive CD4 T cells and expansion of CD8 memory T cells (TEMRAs), in addition to enrichment of cytotoxic CD4 and PD1+ antiviral CD8 T cells with infection. Furthermore, antibodies against both RBD and NP were detected in the participants.

Severe COVID-19 disease during pregnancy has been recently shown to be associated with myeloid and T cell activation in the placenta (Lu-Culligan et al., 2021). Here, we report broad myeloid cell activation in both macrophage subsets with asymptomatic/mild disease, albeit differential outcomes within the two decidual macrophage subsets: HLA-DR^{high} (dMac1, tissue-resident decidual macrophages) and HLA-DR^{low} (dMac2, blood monocyte-derived decidual macrophages) (Vento-Tormo et al., 2018). Although asymptomatic/mild disease resulted in selective loss of the tissue-resident dMac1, we observed an increase in cytokine-producing (*IL1B*+) macrophages. Given the absence of infection in the placenta, this enrichment of cytokine-producing macrophages could be a response to systemic inflammatory cues at the time of acute infection. Both macrophage subsets exhibited elevated signatures of TLR, NF-κB, cytokine, and chemokine signaling, suggesting a heightened activation state. However, the expression of several heat-shock proteins (*HSPA5*, *HSPA6*, *HSPE1*) was only upregulated in dMac1, a potentially protective mechanism to cope with cellular stress at the maternal-fetal interface. Additionally, while viral-sensing pathways (RIG-I signaling) and interferon receptor expression (IFNAR1) were upregulated with asymptomatic/mild disease, interferon signaling module scores were attenuated in monocyte-derived macrophages (dMac2) in the decidua. This observation is in line with several studies on peripheral monocytes from mild/moderate non-gravid subjects, where lower plasma interferon alpha (IFNα) and lower IFN signaling have been linked to attenuated TNF-α and IFNγ in plasma and ensuing cytokine storm. Finally, a reduction in HLA-DR expression and

MHC class II module scores was observed in dMac2, consistent with studies on circulating monocytes with COVID-19 (Schulte-Schrepping et al., 2020; Wilk et al., 2020). Macrophages in the decidua play diverse roles ranging from clearance of apoptotic bodies and wound healing to host defense, pathogen clearance, and initiation of labor. Aberrantly activated macrophages could potentially disrupt these processes and provide a potential mechanism for increased adverse outcomes for pregnant women with COVID-19 (Schwartz et al., 2022).

We report a modest loss of naive T cells and an expansion of memory subsets in both blood and decidua, including PD1+ CD8 T cells. As recently described for patients hospitalized with severe COVID-19 (Lu-Culligan et al., 2021), we detected an expansion of CD8+CD69+ and CD4+CD69+ tissue-resident T cells with asymptomatic/mild disease. We also report a loss of Tregs in decidua but an expansion of HLA-DRA-expressing activated CD4 T cells. Additionally, upregulation of MHC class II molecules on CD8 T cells was reported exclusively in the decidua, whereas the appearance of cytotoxic CD4 T cells expressing *CXCR4* and high levels of *GZMA*, *GZMH*, and *CCL5* was seen only in the blood. In circulation, circulating CD4 T cells showed downregulated signatures of apoptotic signaling, TNF, and IFNγ signaling not observed in the decidua. Finally, T cell repertoire analysis suggests that, unlike in blood, T cells in decidua undergo minimal clonal expansion following asymptomatic infection. Taken together, these findings suggest that while antiviral cytotoxic responses are likely restricted to the blood, activated tissue-resident decidual T cells are expanded with infection and exhibit signs of heightened IFN signaling. These changes in the T cell compartment coupled with the loss of regulatory tissue-resident macrophages (dMac1) may skew the balance of decidual immune cells toward a pro-inflammatory state, thereby contributing to pregnancy complications.

Limitations of the study

The main limitation of this study is the small sample size, which, combined with the wide window of infectivity during pregnancy and the presence of samples from subjects with both asymptomatic and mild disease, precluded the assessment of gestational age and disease severity on immunological outcomes. Given the limited amount of maternal blood obtained, we were unable to conduct a comprehensive measurement of antigen-specific T and B cell responses. Finally, it remains unclear if the placenta harbors virus-specific T cells that migrate from blood. Additionally, certain aspects of COVID-19-associated immune responses at the maternal-fetal interface such as IL-10 expression, antibody transfer, and interferon-stimulated gene (ISG) expression have been shown to be more prominent in mothers carrying male fetuses (Bordt et al., 2021). Given the relatively small sample size of our study, we were unable to dissect fetal sex-specific adaptations in the placenta. Finally, maternal infections have been shown to mildly affect the umbilical cord blood cytokine environment, affecting fetal T cell responses with no dramatic changes in their repertoire diversity (Garcia-Flores et al., 2022; Gee et al., 2021). However, given how sensitive the fetal myeloid compartment is to maternal inflammation, it remains to be seen if asymptomatic/mild maternal infection can have long-term consequences on immunity in the offspring.

STAR★METHODS

Detailed methods are provided in the online version of this paper and include the following:

- KEY RESOURCES TABLE
- RESOURCE AVAILABILITY
  - Lead contact
  - Materials availability
  - Data and code availability
- EXPERIMENTAL MODEL AND SUBJECT DETAILS
- METHOD DETAILS
  - Blood processing
  - PBMC phenotyping
  - Serology
  - Placenta processing
  - Decidua immunophenotyping
  - 3′ multiplexed single-cell RNA sequencing
  - 5′ multiplexed single cell RNA sequencing with feature barcoding
  - Single-cell RNA-Seq data analysis
  - scTCR analysis
- QUANTIFICATION AND STATISTICAL ANALYSIS

SUPPLEMENTAL INFORMATION

Supplemental information can be found online at https://doi.org/10.1016/j.celrep.2022.110938.

ACKNOWLEDGMENTS

We are grateful to all participants in this study. We thank the MFM Research Unit at OHSU for sample collection. We thank Dr. Jennifer Atwood for assistance with sorting at the Flow Cytometry Core at the Institute for Immunology, UCI. We thank the UCI Genomics and High-Throughput Facility for assistance with 10X library sequencing. Aspects of experimental design figures were generated using graphics from Biorender.com. This study was supported by the National Center for Research Resources and the National Center for Advancing Translational Sciences, National Institutes of Health through grants UL1TR001414, 1R01AI142841, and 1R01AI145910. The authors also wish to acknowledge the support of the Chao Family Comprehensive Cancer Center Experimental Tissue Shared Resource, supported by the National Cancer Institute of the NIH under award number P30CA062203. The content is solely the responsibility of the authors and does not necessarily represent the official views of the NIH.

AUTHOR CONTRIBUTIONS

Conceptualization, S.S., N.E.M., and I.M.; methodology, S.S., N.E.M., and I.M.; investigation, S.S., M.Z.Z., B.M.D., and A.J.; writing, S.S. and I.M.; funding acquisition, N.E.M. and I.M.; resources, M.R., D.T., and R.E. All authors have read and approved the final draft of the manuscript.

DECLARATION OF INTERESTS

The authors declare no competing interests.

Received: December 12, 2021
Revised: March 21, 2022
Accepted: May 18, 2022
Published: May 25, 2022

REFERENCES

Afshar, Y., Gaw, S.L., Flaherman, V.J., Chambers, B.D., Krakow, D., Berghella, V., Shamshirsaz, A.A., Boatin, A.A., Aldrovandi, G., Greiner, A., et al. (2020). Clinical presentation of coronavirus disease 2019 (COVID-19) in pregnant and recently pregnant people. Obstet. Gynecol. *136*, 1117–1125. https://doi.org/10.1097/AOG.0000000000004178.

Aghaeepour, N., Ganio, E.A., McIlwain, D., Tsai, A.S., Tingle, M., Van Gassen, S., Gaudilliere, D.K., Baca, Q., McNeil, L., Okada, R., et al. (2017). An immune clock of human pregnancy. Sci. Immunol. *2*, eaan2946. https://doi.org/10.1126/sciimmunol.aan2946.

Aghaeepour, N., Lehallier, B., Baca, Q., Ganio, E.A., Wong, R.J., Ghaemi, M.S., Culos, A., El-Sayed, Y.Y., Blumenfeld, Y.J., Druzin, M.L., et al. (2018). A proteomic clock of human pregnancy. Am. J. Obstet. Gynecol. *218*, 347.e1–347.e14. https://doi.org/10.1016/j.ajog.2017.12.208.

Ander, S.E., Diamond, M.S., and Coyne, C.B. (2019). Immune responses at the maternal-fetal interface. Sci. Immunol. *4*, eaat6114. https://doi.org/10.1126/sciimmunol.aat6114.

Arunachalam, P.S., Wimmers, F., Mok, C.K.P., Perera, R.A.P.M., Scott, M., Hagan, T., Sigal, N., Feng, Y., Bristow, L., Tak-Yin Tsang, O., et al. (2020). Systems biological assessment of immunity to mild versus severe COVID-19 infection in humans. Science *369*, 1210–1220. https://doi.org/10.1126/science.abc6261.

Bordt, E.A., Shook, L.L., Atyeo, C., Pullen, K.M., De Guzman, R.M., Meinsohn, M.C., Chauvin, M., Fischinger, S., Yockey, L.J., James, K., et al. (2021). Maternal SARS-CoV-2 infection elicits sexually dimorphic placental immune responses. Sci. Transl. Med. *13*, eabi7428. https://doi.org/10.1126/scitranslmed.abi7428.

Chen, G., Wu, D., Guo, W., Cao, Y., Huang, D., Wang, H., Wang, T., Zhang, X., Chen, H., Yu, H., et al. (2020). Clinical and immunological features of severe and moderate coronavirus disease 2019. J. Clin. Invest. *130*, 2620–2629. https://doi.org/10.1172/JCI137244.

De Biasi, S., Tartaro, D.L., Gibellini, L., Paolini, A., Quong, A., Petes, C., Awong, G., Douglas, S., Lin, D., Nieto, J., et al. (2021). Endogenous control of inflammation characterizes pregnant women with asymptomatic or paucisymptomatic SARS-CoV-2 infection. Nat. Commun. *12*, 4677. https://doi.org/10.1038/s41467-021-24940-w.

Edlow, A.G., Li, J.Z., Collier, A.R.Y., Atyeo, C., James, K.E., Boatin, A.A., Gray, K.J., Bordt, E.A., Shook, L.L., Yonker, L.M., et al. (2020a). Assessment of maternal and neonatal SARS-CoV-2 viral load, transplacental antibody transfer, and placental pathology in pregnancies during the COVID-19 pandemic. Jama Netw. Open *3*, e2030455. https://doi.org/10.1001/jamanetworkopen.2020.30455.

Edlow, A.G., Li, J.Z., Collier, A.r.Y., Atyeo, C., James, K.E., Boatin, A.A., Gray, K.J., Bordt, E.A., Shook, L.L., Yonker, L.M., et al. (2020b). Assessment of maternal and neonatal SARS-CoV-2 viral load, transplacental antibody transfer, and placental pathology in pregnancies during the COVID-19 pandemic. Jama Netw. Open *3*, e2030455, ARTN e2030455. https://doi.org/10.1001/jamanetworkopen.2020.30455.

Garcia-Flores, V., Romero, R., Xu, Y., Theis, K., Arenas-Hernandez, M., Miller, D., Peyvandipour, A., Galaz, J., Levenson, D., Bhatti, G., et al. (2021). Maternal-fetal immune responses in pregnant women infected with SARS-CoV-2. Res. Sq. *13*, 320. https://doi.org/10.21203/rs.3.rs-362886/v1.

Garcia-Flores, V., Romero, R., Xu, Y., Theis, K.R., Arenas-Hernandez, M., Miller, D., Peyvandipour, A., Bhatti, G., Galaz, J., Gershater, M., et al. (2022). Maternal-fetal immune responses in pregnant women infected with SARS-CoV-2. Nat. Commun. *13*, 320. https://doi.org/10.1038/s41467-021-27745-z.

Gee, S., Chandiramani, M., Seow, J., Pollock, E., Modestini, C., Das, A., Tree, T., Doores, K.J., Tribe, R.M., and Gibbons, D.L. (2021). The legacy of maternal SARS-CoV-2 infection on the immunology of the neonate. Nat. Immunol. *22*, 1490–1502. https://doi.org/10.1038/s41590-021-01049-2.

Hojyo, S., Uchida, M., Tanaka, K., Hasebe, R., Tanaka, Y., Murakami, M., and Hirano, T. (2020). How COVID-19 induces cytokine storm with high mortality. Inflamm. Regen. *40*, 37, ARTN 37. https://doi.org/10.1186/s41232-020-00146-3.

Hsieh, L.E., Grifoni, A., Dave, H., Wang, J., Johnson, D., Zellner, J., Sidney, J., Chambers, C., and Franco, A. (2022). SARS-CoV-2-specific T cell responses and immune regulation in infected pregnant women. J. Reprod. Immunol. *149*, 103464. https://doi.org/10.1016/j.jri.2021.103464.

Huang, C., Wang, Y., Li, X., Ren, L., Zhao, J., Hu, Y., Zhang, L., Fan, G., Xu, J., Gu, X., et al. (2020). Clinical features of patients infected with 2019 novel coronavirus in Wuhan, China. Lancet *395*, 497–506. https://doi.org/10.1016/S0140-6736(20)30183-5.

Jamieson, D.J., Theiler, R.N., and Rasmussen, S.A. (2006). Emerging infections and pregnancy. Emerg. Infect. Dis. *12*, 1638–1643. https://doi.org/10.3201/eid1211.060152.

Kourtis, A.P., Read, J.S., and Jamieson, D.J. (2014). Pregnancy and infection. N. Engl. J. Med. *370*, 2211–2218. https://doi.org/10.1056/nejmra1213566.

Laing, A.G., Lorenc, A., Del Molino Del Barrio, I., Das, A., Fish, M., Monin, L., Munoz-Ruiz, M., McKenzie, D.R., Hayday, T.S., Francos-Quijorna, I., et al. (2020). A dynamic COVID-19 immune signature includes associations with poor prognosis. Nat. Med. *26*, 1623–1635. https://doi.org/10.1038/s41591-020-1038-6.

Li, N., Han, L., Peng, M., Lv, Y., Ouyang, Y., Liu, K., Yue, L., Li, Q., Sun, G., Chen, L., and Yang, L. (2020). Maternal and neonatal outcomes of pregnant women with coronavirus disease 2019 (COVID-19) pneumonia: a case-control study. Clin. Infect. Dis. *71*, 2035–2041. https://doi.org/10.1093/cid/ciaa352.

Lokken, E.M., Walker, C.L., Delaney, S., Kachikis, A., Kretzer, N.M., Erickson, A., Resnick, R., Vanderhoeven, J., Hwang, J.K., Barnhart, N., et al. (2020). Clinical characteristics of 46 pregnant women with a severe acute respiratory syndrome coronavirus 2 infection in Washington State. Am. J. Obstet. Gynecol. *223*, 911.e1–911.e14, ARTN 911.e1-e14. https://doi.org/10.1016/j.ajog.2020.05.031.

Lu-Culligan, A., Chavan, A.R., Vijayakumar, P., Irshaid, L., Courchaine, E.M., Milano, K.M., Tang, Z., Pope, S.D., Song, E., Vogels, C.B.F., et al. (2021). SARS-CoV-2 infection in pregnancy is associated with robust inflammatory response at the maternal-fetal interface. Preprint at medRxiv. https://doi.org/10.1101/2021.01.25.21250452.

Lucas, C., Wong, P., Klein, J., Castro, T.B.R., Silva, J., Sundaram, M., Ellingson, M.K., Mao, T., Oh, J.E., Israelow, B., et al. (2020). Longitudinal analyses reveal immunological misfiring in severe COVID-19. Nature *584*, 463–469. https://doi.org/10.1038/s41586-020-2588-y.

Delahoy, M.J., Whitaker, M., O'Halloran, A., Chai, S.J., Kirley, P.D., Alden, N., Kawasaki, B., Meek, J., Yousey-Hindes, K., Anderson, E.J., et al. (2020). Characteristics and maternal and birth outcomes of hospitalized pregnant women with laboratory-confirmed COVID-19 — COVID-NET, 13 states, March 1–August 22, 2020. MMWR Morb. Mortal. Wkly. Rep. *69*, 1347–1354. https://doi.org/10.15585/mmwr.mm6938e1.

Sappenfield, E., Jamieson, D.J., and Kourtis, A.P. (2013). Pregnancy and susceptibility to infectious diseases. Infect. Dis. Obstet. Gynecol. *2013*, 752852. https://doi.org/10.1155/2013/752852.

Schulte-Schrepping, J., Reusch, N., Paclik, D., Baßler, K., Schlickeiser, S., Zhang, B., Kramer, B., Krammer, T., Brumhard, S., Bonaguro, L., et al. (2020). Severe COVID-19 is marked by a dysregulated myeloid cell compartment. Cell *182*, 1419–1440.e23. https://doi.org/10.1016/j.cell.2020.08.001.

Schwartz, D.A., Avvad-Portari, E., Babal, P., Baldewijns, M., Blomberg, M., Bouachba, A., Camacho, J., Collardeau-Frachon, S., Colson, A., Dehaene, I., et al. (2022). Placental tissue destruction and insufficiency from COVID-19 causes stillbirth and neonatal death from hypoxic-ischemic injury: a study of 68 cases with SARS-CoV-2 placentitis from 12 countries. Arch. Pathol. Lab. Med. *146* (6), 660–676. https://doi.org/10.5858/arpa.2022-0029-SA.

Schwartz, D.A., and Morotti, D. (2020). Placental pathology of COVID-19 with and without fetal and neonatal infection: trophoblast necrosis and chronic histiocytic intervillositis as risk factors for transplacental transmission of SARS-CoV-2. Viruses *12*, 1308. https://doi.org/10.3390/v12111308.

Subbaraman, N. (2021). Pregnancy and COVID: what the data say. Nature *591*, 193–195. https://doi.org/10.1038/d41586-021-00578-y.

van der Zwan, A., Bi, K., Norwitz, E.R., Crespo, A.C., Claas, F.H.J., Strominger, J.L., and Tilburgs, T. (2018). Mixed signature of activation and dysfunction allows human decidual CD8(+) T cells to provide both tolerance and immunity. Proc. Natl. Acad. Sci. U S A *115*, 385–390. https://doi.org/10.1073/pnas.1713957115.

Vento-Tormo, R., Efremova, M., Botting, R.A., Turco, M.Y., Vento-Tormo, M., Meyer, K.B., Park, J.E., Stephenson, E., Polanski, K., Goncalves, A., et al. (2018). Single-cell reconstruction of the early maternal-fetal interface in humans. Nature *563*, 347–353. https://doi.org/10.1038/s41586-018-0698-6.

Verma, S., Joshi, C.S., Silverstein, R.B., He, M., Carter, E.B., and Mysorekar, I.U. (2021). SARS-CoV-2 colonization of maternal and fetal cells of the human placenta promotes alteration of local renin-angiotensin system. Med *2*, 575–590.e5. https://doi.org/10.1016/j.medj.2021.04.009.

Villar, J., Ariff, S., Gunier, R.B., Thiruvengadam, R., Rauch, S., Kholin, A., Roggero, P., Prefumo, F., do Vale, M.S., Cardona-Perez, J.A., et al. (2021). Maternal and neonatal morbidity and mortality among pregnant women with and without COVID-19 infection the INTERCOVID multinational Cohort study. JAMA Pediatr. *175*, 817. https://doi.org/10.1001/jamapediatrics.2021.1050.

Vivanti, A.J., Vauloup-Fellous, C., Prevot, S., Zupan, V., Suffee, C., Do Cao, J., Benachi, A., and De Luca, D. (2020). Transplacental transmission of SARS-CoV-2 infection. Nat. Commun. *11*, 3572. https://doi.org/10.1038/s41467-020-17436-6.

Wang, X., Wang, D., and He, S. (2020). The role of a cytokine storm in severe coronavirus disease 2019 in pregnancy. Am. J. Obstet. Gynecol. *223*, 780–782. https://doi.org/10.1016/j.ajog.2020.07.010.

Wilk, A.J., Rustagi, A., Zhao, N.Q., Roque, J., Martinez-Colon, G.J., McKechnie, J.L., Ivison, G.T., Ranganath, T., Vergara, R., Hollis, T., et al. (2020). A single-cell atlas of the peripheral immune response in patients with severe COVID-19. Nat. Med. *26*, 1070–1076. https://doi.org/10.1038/s41591-020-0944-y.

Yap, M., Debenham, L., Kew, T., Chatterjee, S.R., Allotey, J., Stallings, E., Coomar, D., Lee, S.I., Qiu, X., Yuan, M., et al. (2020). Clinical manifestations, prevalence, risk factors, outcomes, transmission, diagnosis and treatment of COVID-19 in pregnancy and postpartum: a living systematic review protocol. BMJ Open *10*, e041868. https://doi.org/10.1136/bmjopen-2020-041868.

STAR★METHODS

KEY RESOURCES TABLE

REAGENT or RESOURCE	SOURCE	IDENTIFIER
Antibodies		
CD3-FITC	BD Pharmigen	Cat#556611 Clone-SP34
CD20-FITC	Biolegend	Cat#302304 Clone-2H7
CD56-BV711	Biolegend	Cat#318336 Clone-HCD56
CD57-PE-Cy7	Biolegend	Cat#359624 Clone-HNK-1
KLRG1-APC	Biolegend	Cat# 367716 Clone-SA231a2
CD16-PB	Biolegend	Cat#302032 Clone-3G8
CD14-AF700	Biolegend	Cat#301822 Clone-M5E2
HLA-DR-APC-Cy7	Biolegend	Cat#307618 Clone-L243
CD11c-PE-eF610	ThermoFisher Scientific	Cat#61-0116-42 Clone-3.9
CD123-PCP-Cy5.5	Biolegend	Cat#306016 Clone-6H6
CD86-BV605	Biolegend	Cat#305430 Clone-IT2.2
CD4-APC-Cy7	Biolegend	Cat#317418 Clone-OKT4
CD8b-ECD	Beckman Coulter	Cat#6607123 Clone-2ST8.5H7
CD45RA-PerCP-Cy5.5	TONBO Biosciences	Cat#65-040458-t100 Clone-HI100
CCR7-PE-Cy7	Biolegend	Cat#353226 Clone-GO43H7
CD19-PE	Biolegend	Cat#302208 Clone-HIB19
IgD-BV605	Biolegend	Cat#348232 Clone-IA6-2
CD27-BV711	Biolegend	Cat#356430 Clone-M-T271
PD-1-BV510	Biolegend	Cat#329932 Clone-Eh12.2h7
CD45- FITC	Biolegend	Cat#368501 Clone-HI30
CD66b-FITC	Biolegend	Cat#305104 Clone-G10F5
CD3-PE	BD Pharmigen	Cat#556612 Clone-SP34
Total-seq-C0072-CD4	Biolegend	Cat#300567 Clone-RPA-T4
Total-seq-C0046-CD8	Biolegend	Cat#344753 Clone-SK1

(*Continued on next page*)

Continued

REAGENT or RESOURCE	SOURCE	IDENTIFIER
Total-seq-C0148-CCR7	Biolegend	Cat#353251 Clone-G043H7
Total-seq-C0063-CD45RA	Biolegend	Cat#304163 Clone-HI100
Total-seq-C0146-CD69	Biolegend	Cat#310951 Clone-FN50
Total-seq-C0145-CD103	Biolegend	Cat#350233 Clone-Ber-ACT8
Total-seq-C0088-PD-1	Biolegend	Cat#329963 Clone-EH12.2H7
Total-seq-C0085-CD25	Biolegend	Cat#302649 Clone-BC96
Total-seq-C0251	Biolegend	Cat#394661 Clone- LNH-94, 2M2
Total-seq-C0254	Biolegend	Cat#394667 Clone- LNH-94, 2M2
Total-seq-C0256	Biolegend	Cat#394671 Clone- LNH-94, 2M2
Total-seq-C0260	Biolegend	Cat#394679 Clone- LNH-94, 2M2
Human IgG	BD Pharmigen	Cat#55788 Clone-G17-4
Biological samples		
Fetal Bovine Serum, USDA Certified, Heat Inactivated	Omega Scientific	Cat#FB-02
FetalPlex™ Animal Serum Complex	GeminiBio	Cat#100-602
Chemicals, peptides, and recombinant proteins		
SARS-CoV-2 Spike Protein	Genscript	Cat#Z03483-1
SARS-CoV-2 Nucleocapsid protein	Genscript	Cat# Z03480-1
o-phenylenediamine dihydrochloride	ThermoFisher Scientific	Cat# 34005
Collagenase	Sigma	Cat# C9722 Source: *Clostridium histolyticum*
Percoll Density Gradient	Neta Scientific	Cat# 17-0891-01
Ghost Dye 540	TONBO Biosciences	Cat#13-0879
SYTOX Red Dead Cell Stain	ThermoFisher Scientific	Cat#S34859
SYTOX Blue Dead Cell Stain	ThermoFisher Scientific	Cat#S34857
Human TruStain FcX	Biolegend	Cat# 422302
Bovine Serum Albumin (BSA), Fraction V—Molecular Biology Grade	GeminiBio	Cat#700-106P
Critical commercial assays		
3′ CellPlex Kit Set A	10X Genomics	PN-1000261
Chromium Single Cell 3' Reagent Kits v3	10X Genomics	PN-1000075
3′ Feature Barcode Kit	10X Genomics	PN-1000262
Chromium Single Cell 5' Reagent Kits V2	10X Genomics	PN-1000263
5′ Feature Barcode Kit	10X Genomics	PN-1000256
Deposited data		
3′ Single Cell GEX data	This paper	NCBI Sequence Read Archive: PRJNA817521
5′ Single Cell TCR data	This paper	NCBI Sequence Read Archive: PRJNA817521

(*Continued on next page*)

Continued

REAGENT or RESOURCE	SOURCE	IDENTIFIER
Software and algorithms		
Prism	GraphPad	Version#8
CellRanger	10X Genomics	Version#6.0.2
Seurat	R package	Version#3.1.5
Immunarch	R package	Version#0.6.7
Metascape	www.metascape.org	
ggplot2	R package	Version#3.3.3
Gplots	R package	Version#3.1.1
Attune NxT Flow Cytometer Software	ThermoFisher Scientific	Version#2.5

RESOURCE AVAILABILITY

Lead contact

Further information and requests for resources and reagents should be directed to and will be fulfilled by the lead contact, Dr. Ilhem Messaoudi (ilhem.messaoudi@uky.edu).

Materials availability

This study did not generate new unique reagents.

Data and code availability

- Single-cell RNA-seq data have been deposited at GEO and are publicly available as of the date of publication. Accession numbers are listed in the key resources table.
- This paper does not report original code.
- Additional Supplemental Items are available from Mendeley Data at https://doi.org/10.17632/pxgb3cnxvd.1.
- Any additional information required to reanalyze the data reported in this paper is available from the lead contact upon request.

EXPERIMENTAL MODEL AND SUBJECT DETAILS

This study was approved by the University of California Irvine Institutional Review Boards (Protocol ID HS# 2012-8716) and Oregon and Health Sciences University (eIRB# 22713 and 16328). Informed consent was obtained from all enrolled subjects. All participants in this study were healthy and did not report any significant comorbidities or complications with pregnancy. Detailed characteristics of participants and experimental breakdown by samples are provided in Table S1. Subjects with the asymptomatic disease are defined as those who tested positive during the mandatory screening at the time of admission to labor and delivery. Subjects with mild disease are defined as those who experienced (self-reported) symptoms consistent with mild upper respiratory tract infection but did not necessitate a hospital visit or stay or treatment.

METHOD DETAILS

Blood processing

Whole blood samples were collected in EDTA vacutainer tubes. PBMC and plasma samples were isolated after whole blood centrifugation 1200 g for 10 min at room temperature in SepMate tubes (STEMCELL Technologies). Plasma was stored at -80°C until analysis. PBMC were cryo-preserved using 10% DMSO/FBS and Mr. Frosty Freezing containers (Thermo Fisher Scientific) at -80C then transferred to a cryogenic unit 24 h later until analysis.

PBMC phenotyping

Frozen PBMCs were thawed, washed in FACS buffer (2% FBS, 1 mM EDTA in PBS), and counted on TC20 (Biorad) before surface staining using two independent flow panels. For the innate panel, the following antibodies were used: CD3 (SP34, BD Pharmingen) and CD20 (2H7, BioLegend) for the exclusion of T & B lymphocytes, respectively. We further stained for CD56 (HCD56, Biolegend), CD57 (HNK-1, BioLegend), KLRG1 (SA231A2, BioLegend) CD16 (3G8, BioLegend), CD14 (M5E2, BioLegend), HLA-DR (L243, BioLegend), CD11c (3.9, ThermoFisher Scientific), CD123 (6H6, BioLegend) and CD86 (IT2.2, BioLegend). For the adaptive panel, the following antibodies were used: CD4 (OKT4, BioLegend), CD8b (2ST8.5H7, Beckman Coulter), CD45RA (HI100, TONBO Biosciences), CCR7 (G043H7, Biolegend), CD19 (HIB19, BioLegend), IgD (IA6-2, BioLegend), CD27 (M-T271, BioLegend), KLRG1 (SA231A2, BioLegend) and PD-1 (Eh12.2h7, BioLegend). Cells were stained with Ghost Dye viability dye (TONBO biosciences) for

30 min at 4C per manufacturer's instructions, washed, surface stained with either innate or adaptive panels for 30 min at 4C. Samples were then washed and analyzed on Attune NxT Flow Cytometer (ThermoFisher Scientific, Waltham MA).

Serology

RBD and NP end-point titers were determined using standard ELISA and plates coated with 500 ng/mL SARS-CoV-2 Spike-protein Receptor-Binding Domain (RBD) (GenScript, Piscataway NJ) or 1ug/mL SARS-CoV-2 nucleocapsid protein (NP). Heat inactivated plasma was added in 3-fold dilutions starting at 1:50. Responses were visualized by adding HRP-anti-human IgG (BD Pharmingen) followed by the addition of o-phenylenediamine dihydrochloride (ThermoFisher Scientific). ODs were read at 490 nm on a Victor3^{TM} Multilabel plate reader (Perkin Elmer). Batch differences were minimized by normalizing to positive control samples run on each plate.

Placenta processing

Decidua basalis and villous chorion membranes were separated and immediately immersed in RPMI supplemented with 10% FBS and antibiotics. Samples were processed within 24 h of collection. Decidua basalis membranes were washed thoroughly in HBSS to remove contaminating blood. Tissues were minced into approximately 0.2–0.3 mm^3 cubes and enzymatically digested in 0.5 mg/mL collagenase V (Sigma, C-9722) solution in 50 mL R3 media (RPMI 1640 with 3% FBS, 1% Penicillin-Streptomycin, 1% L-glutamine, and 1M HEPES) at 37C for 1 h. The disaggregated cell suspension was passed through tissue strainers to eliminate large tissue chunks. Cells were pelleted from the filtrate, passed through 70-um cell sieve, centrifuged, and resuspended in R3 media. Red blood cells were lysed using RBC lysis buffer (155 mM NH_4Cl, 12 mM $NaHCO_3$, 0.1 mM EDTA in double-distilled water) and resuspended in 5 mL R3 media. The cell suspension was then layered on a discontinuous 60% and 40% percoll gradient and centrifuged for 30 min with brakes off. Immune cells at the interface of 40% and 60% gradients were collected, washed in HBSS, counted, and cryopreserved for future analysis.

Decidua immunophenotyping

1-2 X 10^6 fresh decidual leukocytes were washed with PBS and stained using the following cocktail of antibodies: CD45 (HI30, Biolegend), CD66b (G10F5, BioLegend), CD20 (2H7, BioLegend), CD4 (OKT4, BioLegend), CD8b (2ST8.5H7, Beckman Coulter), CD14 (M5E2, BioLegend), HLA-DR (L243, BioLegend), CD56 (HCD56, Biolegend), CD16 (3G8, BioLegend), CD11c (3.9, ThermoFisher Scientific), CD123 (6H6, BioLegend), for 20 min in dark at 4C. Samples were washed twice in FACS buffer and resuspended in 400 uL. All samples were acquired with the Attune NxT Flow Cytometer (ThermoFisher Scientific, Waltham MA), immediately after addition of SYTOX Red Dead Cell Stain (1:1000). Data were analyzed using FlowJO (Ashland OR).

3′ multiplexed single-cell RNA sequencing

Freshly thawed decidual immune cells (1-2 $10e^6$ cells) were incubated with Fc blocker (Human TruStain FcX, Biolegend) in PBS with 1% BSA for 10 min at 4C and then surface stained with CD45-FITC (HI30, Biolegend) for 30 min in the dark. Samples were then washed twice in PBS with 0.04% BSA and incubated with individual 3′ CellPlex oligos (10X Genomics) per manufacturer's instructions for 5 min at room temperature. Pellets were washed three times in PBS with 1% BSA, resuspended in 300 uL FACS buffer, and sorted on BD FACS Aria Fusion into RPMI (supplemented with 30% FBS) following the addition of SYTOX Blue stain for live versus dead discrimination. Sorted live cells were counted in triplicates on a TC20 Automated Cell Counter (BioRad), washed, and resuspended in PBS with 0.04% BSA in a final concentration of 1500 cells/uL. Single cell suspensions were then immediately loaded on the 10X Genomics Chromium Controller with a loading target of 20,000 cells. Libraries were generated using the V3 chemistry (for gene expression) and Single Cell 3' Feature Barcode Library Kit per the manufacturer's instructions (10X Genomics, Pleasanton CA). Libraries were sequenced on Illumina NovaSeq with a sequencing target of 30,000 gene expression reads and 5,000 multiplexed CellPlex reads per cell.

5′ multiplexed single cell RNA sequencing with feature barcoding

Matched PBMC and decidual leukocytes were thawed, washed, filtered, and stained with Ghost Violet 540 live-dead stain (Tonbo Biosciences) for 30 min in the dark at 4C. Given the parallel assessment of both TCR and gene expression, we used an antibody-based multiplexing technology as it is the only compatible with 5′ gene expression analysis. Samples were washed thoroughly with a cell staining buffer (1X PBS with 0.5% BSA), and Fc blocked for 10 min (Human TruStain FcX, Biolegend), and incubated with a cocktail containing CD3-PE (SP34, BD Pharmingen), 0.5 ug each of oligo tagged CD4 (TotalSeq^{TM}-C0072, Biolegend), CD8 (TotalSeq^{TM}-C0046, Biolegend), CCR7 (TotalSeq^{TM}-C0148, Biolegend), CD45RA (TotalSeq^{TM}-C0063, Biolegend), CD69 (TotalSeq^{TM}-C0146, Biolegend), CD103 (TotalSeq^{TM}-C0145, Biolegend), PD-1(TotalSeq^{TM}-C0088, Biolegend), CD25 (TotalSeq^{TM}-C0085, Biolegend), and unique 5′ hashing antibody (TotalSeq^{TM}-C0251, C0254, C0256, and C0260, Biolegend) for an additional 30 min at 4C. Samples were washed four times with 1X PBS (serum and azide free), filtered using Flowmi 1000 uL pipette strainers (SP Bel-Art) and resuspended in 300 uL FACS buffer. CD3+ T cells were sorted on the BD FACS Aria Fusion into RPMI (supplemented with 30% FBS). Sorted pellets were counted in triplicates on a TC20 Automated Cell Counter (BioRad), washed and resuspended in PBS with 0.04% BSA in a final concentration of 1500 cells/uL. Single cell suspensions were then immediately loaded on the 10X Genomics Chromium Controller with a loading target of 20,000 cells. Libraries were generated using the 5′ V2 chemistry (for gene expression) and Single Cell 5' Feature Barcode Library Kit per manufacturer's instructions (10X Genomics, Pleasanton CA). Libraries

were sequenced on Illumina NovaSeq with a sequencing target of 30,000 gene expression reads and 10,000 multiplexed CellPlex reads per cell.

Single-cell RNA-Seq data analysis

For 3′ gene expression with CellPlex, raw reads were aligned and quantified using Cell Ranger (version 6.0.2, 10X Genomics) against the human reference genome (GRCh38) using the *multi* option and CMO information. Only singlets identified from each sample were included in downstream analyses. For 5′ gene expression, alignments were performed using the *feature* and *vdj* option in Cell Ranger. Following alignment, hashing (HTO) and cell surface features (Antibody Capture) from feature barcoding alignments were manually updated in cellranger generated features file. Doublets were then removed in Seurat using the *HTODemux* function, which assigned sample identity to every cell in the matrix. Droplets with ambient RNA (cells with fewer than 400 detected genes), and dying cells (cells with more than 20% total mitochondrial gene expression) were excluded during initial QC. Data normalization and variance stabilization were performed on the integrated object using the *NormalizeData* and *ScaleData* functions in Seurat where a regularized negative binomial regression corrected for differential effects of mitochondrial and ribosomal gene expression levels. Dimension reduction was performed using *RunPCA* function to obtain the first 30 principal components and clusters visualized using Seurat's *RunUMAP* function. Cell types were assigned to individual clusters using *FindMarkers* function with a $\log_2$ fold change cutoff of at least 0.4 (FDR<0.05) and using a known catalog of well-characterized scRNA markers for human PBMC and decidual leukocytes. For T cells, 5′ feature barcoding reads were normalized using centered logratio (CLR) transformation. Differential markers between clusters were then detected using *FindMarkers* function. A combination of gene expression and protein markers was used to define T cell subsets. CCR7 staining did not exhibit a significant positive peak, and hence was excluded from all downstream analyses. A list of cluster specific markers is provided in Tables S2, S3, and S4. Differential expression analysis was performed using the wilcoxon rank-sum test using default settings in Seurat. Only statistically significant genes ($\log_{10}$(fold change) cutoff $\geq$ 0.4; adjusted p-value $\leq$ 0.05) were included in downstream analyses. Module scores for specific gene sets were incorporated cluster-wise using *AddModuleScores* function.

scTCR analysis

TCR reads were aligned to VDJ-GRCh38 ensembl reference using Cell Ranger 6.0 (10X Genomics) generating sequences and annotations such as gene usage, clonotype frequency, and cell-specific barcode information. Only cells with one productive alpha and/or one productive beta chain were retained for downstream analyses. CDR3 sequences were required to have a length between 5 and 27 amino acids, start with a C, and not contain a stop codon. Clonal assignments from cellranger were used to perform all downstream analyses using the R package immunarch. Data were first parsed through *repLoad* function in immunarch, and clonality was examined using *repExplore* function. Family and allele level distributions of TRA and TRB genes were computed using *geneUsage* function. Diversity estimates (Hill numbers) were calculated using *repDiversity* function.

QUANTIFICATION AND STATISTICAL ANALYSIS

Data sets were first tested for normality using the Shapiro-Wilk test. Two-way comparisons for normally distributed data were tested for significance using an unpaired t-test with Welch's correction. For comparisons involving multiple groups, differences were tested using one-way ANOVA followed by Holm Sidak's multiple comparisons tests. p values less than or equal to 0.05 were considered statistically significant. Values between 0.05 and 0.1 are reported as trending patterns.